PROJECTILE COMPOSITIONS AND MODAL FREQUENCIES ON THE "CHEMISTRY OF MICROMETEOROIDS" LDEF EXPERIMENT

Ronald P. Bernhard, Thomas H. See
Lockheed Engineering & Science Company
Houston, Texas 77058
(713) 483-5018/5027 / FAX (713) 483-5347

and

Friedrich Hörz
NASA / Johnson Space Center
Houston, Texas 77058
(713) 483-5042 / FAX (713) 483-5347

SUMMARY

The Chemistry of Micrometeoroids Experiment (LDEF instrument A0187-1) exposed witness plates of high-purity gold (>99.99% Au) and commercial aluminum (>99% Al) with the objective of analyzing the residues of cosmic-dust and orbital-debris particles associated with hypervelocity impact craters. The gold substrates were located ~8^0 off LDEF's trailing edge (Bay A03), while the aluminum surfaces resided in Bay A11, ~52^0 from LDEF's leading edge.

SEM-EDX techniques were employed to analyze the residues associated with 199 impacts on the gold and 415 impacts on the aluminum surfaces. The residues that could be analyzed represent natural or man-made materials. The natural particles dominate at all particle sizes >5 μm. It is possible to subdivide both particle populations into subclasses. Chondritic compositions dominate the natural impactors (71%), followed by monomineralic, mafic-silicate compositions (26%), and by Fe-Ni rich sulfides (~3%). Approximately 30% of all craters on the gold collectors were caused by man-made debris such as aluminum, paint flakes, and other disintegrated, structural and electronic components. Equations-of-state and associated calculations of shock stresses for typical LDEF impacts into the gold and aluminum substrates suggest that substantial vaporization may have occurred during many of the impacts, and is the reason why ~50% of all craters did not contain sufficient residue to permit analysis by the SEM-EDX technique.

After converting the crater diameters into projectile sizes using encounter speeds typical for the trailing-edge and forward-facing (Row 11) directions, and accounting for normalized exposure conditions of the CME collectors, we derived the absolute and relative fluxes of specific projectile classes. The natural impactors encounter all LDEF pointing directions with comparable, modal frequencies suggesting compositional (and dynamic) homogeneity of the interplanetary-dust environment in near-Earth orbit.

INTRODUCTION

The Chemistry of Micrometeoroids Experiment (CME) exposed two substantially different instruments, one active, the other passive (ref. 1). The active experiment consisted of clamshell-type devices that could be opened and closed such that the collectors were protected against contamination during all ground handling and LDEF deployment. This experiment exposed ~0.82 m^2 of high-purity gold (>99.99%) on LDEF's trailing-edge (*i.e.*, Bay A03). The actual collectors consisted of seven individual panels (~20 x 57 cm each) ~0.5 mm thick. The Au collectors exhibited relatively low crater densities because (1) of the specific pointing direction (*i.e.*, trailing edge) which inherently yields the smallest particle flux (ref. 2), and (2) the collectors were only exposed for a total of 3.4 years (refs. 1 and 3). In contrast, the passive experiment (Bay A11) continuously exposed ~1.1 m^2 of aluminum (commercial series 1100, annealed; >99% Al) for the entire 5.7 years in which LDEF was in low-Earth orbit (LEO). Six individual panels (~41 x 46 cm, each) ~3.2 mm thick made up the exposed collector surface for this forward-facing experiment. We previously reported on the detailed optical examinations of these surfaces to determine projectile size-frequency distributions and spatial densities; this earlier report also included some preliminary assessment of the compositional nature of a small set of impactors (ref. 1).

The present report focuses on our subsequent efforts to produce statistically meaningful assessments of the compositional variability of hypervelocity particles in LEO. We have now surveyed all craters >30 μm in diameter on the Au-collectors, as well as a randomly selected suite of smaller impacts, ~10-30 μm in size, resulting in a total of 199 craters. Therefore, the results are complete for all "large" craters on the trailing-edge instrument. To date, we have completed chemical analysis of all 415 craters >75 μm in diameter on two of the six aluminum panels. This latter suite is believed to be representative of the "large" crater population on the forward-facing aluminum collectors.

In general, we followed the analytical procedures and compositional particle classifications developed during the analysis of interplanetary dust recovered from the stratosphere (refs. 4 and 5), or of space retrieved surfaces such as Solar Maximum Mission replacement parts (refs. 6 and 7), or the Palapa satellite (ref. 8). The present effort specifically adds to previous work by analyzing a much larger number of events and by being able to place them into a dynamic dust environment, since LDEF was gravity-gradient stabilized, while all previously analyzed surfaces originated from spin-stabilized spacecraft. Unlike spin-stabilized satellites, LDEF offers the potential to yield substantial directional information (*e.g.*, refs. 2, 9, 10, 11, and 12).

ANALYTICAL METHOD AND GENERAL OBSERVATIONS

An ISI-SR50 Scanning Electron Microscope (SEM) was employed to collect energy dispersive X-Ray (EDX) spectra using a Si(Li) detector on a LINK eXL analyzer with the detector arranged at 90° to the beam path. Although we characterize our analyses as qualitative

and of a survey-type nature, we spent considerable efforts in optimizing the signal to noise ratio of the X-Ray spectra. Initially it was found that an uncomfortably large fraction of craters yield spectra that contained no detectable signal above that of the background. Therefore, we used a number of craters to investigate a range of electron-beam geometries (diameter and take-off angle), low- and high-beam voltage, and widely variable count times (minutes to hours). From these efforts it was determined that a relatively high-beam voltage (25-20 KeV) and long count times (500-1000 seconds) with the specimen tilted at 30° yielded the best results. It is our belief that high-beam voltages are best because the surface relief of the crater interiors tends to be uneven permitting excitation of more near-surface specimen volume compared to less penetrative, low-energy electrons. Count times in excess of 1000 seconds do not appreciably improve signal to noise ratios and do not warrant the additional expenditure of resources.

Generally, contamination of our surfaces was not a problem because the composition of such contamination tends to differ dramatically from that of the projectile residues. Nevertheless, we have observed Si-Ca rich deposits, presumably outgassed RTV (ref. 13) in some crater interiors. Interestingly, such deposits can have distinctly asymmetric distributions in some craters, substantiating the macroscopic LDEF observations of highly directional flow of gaseous contaminants and their condensates. We also observe some intrinsic, heterogeneously distributed contaminants, the result of manufacturing procedures in our collector materials, most notably As in the gold and Si in the aluminum. There is no question that contamination can be a nuisance, but we do not think that it affects the recognition of discrete compositional groupings of projectile types, the major objective of this work.

For many individual craters one may obtain different spectra, especially for those craters that possess mixtures of molten material and unmelted fragments. The latter yield spectra consistent with component minerals of dust grains (*e.g.*, olivines or pyroxenes) that differ distinctly from the melted bulk-residue. However, variability within the pure melts was observed with the largest variations occurring in those craters that contained unmelted residues, suggesting the presence of incompletely mixed mineral melts (refs. 14 and 15). Generally, this melt variability relates to subtly different elemental ratios among different spectra obtained from the same specimen. Nevertheless, this specimen heterogeneity does not affect our classification into natural and man-made particle sources, nor the assignment to a specific compositional subclass.

Our observations for the Au collectors have been summarized in a catalog that contains an SEM image of each crater, its diameter, a typical EDX-spectrum, and our tentative assignment of particle origin and subclass (ref. 16). A less polished compilation is being maintained for the aluminum surfaces that contains ~400 entries which are summarized here. However, it should be noted that aluminum impactors cannot be detected on a substrate composed of aluminum, like that used on the forward-facing A11 collectors.

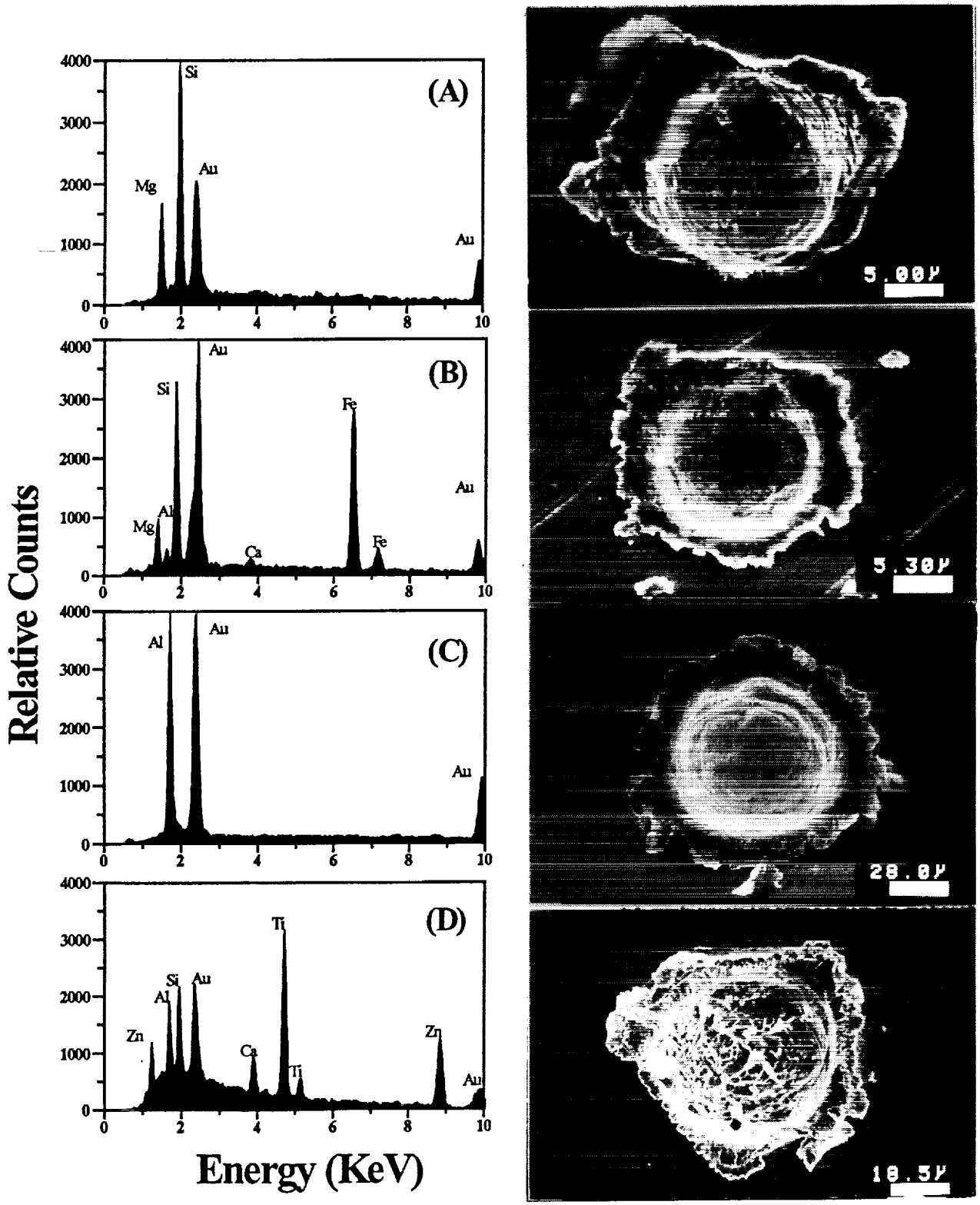

FIGURES 1A - 1D. Representative morphologies of hypervelocity impact craters and associated X-Ray spectra for natural and man-made projectile residues. Figures on this page portray observations from the trailing-edge gold collectors (LDEF Bay A03). For detailed descriptions and comments see text.

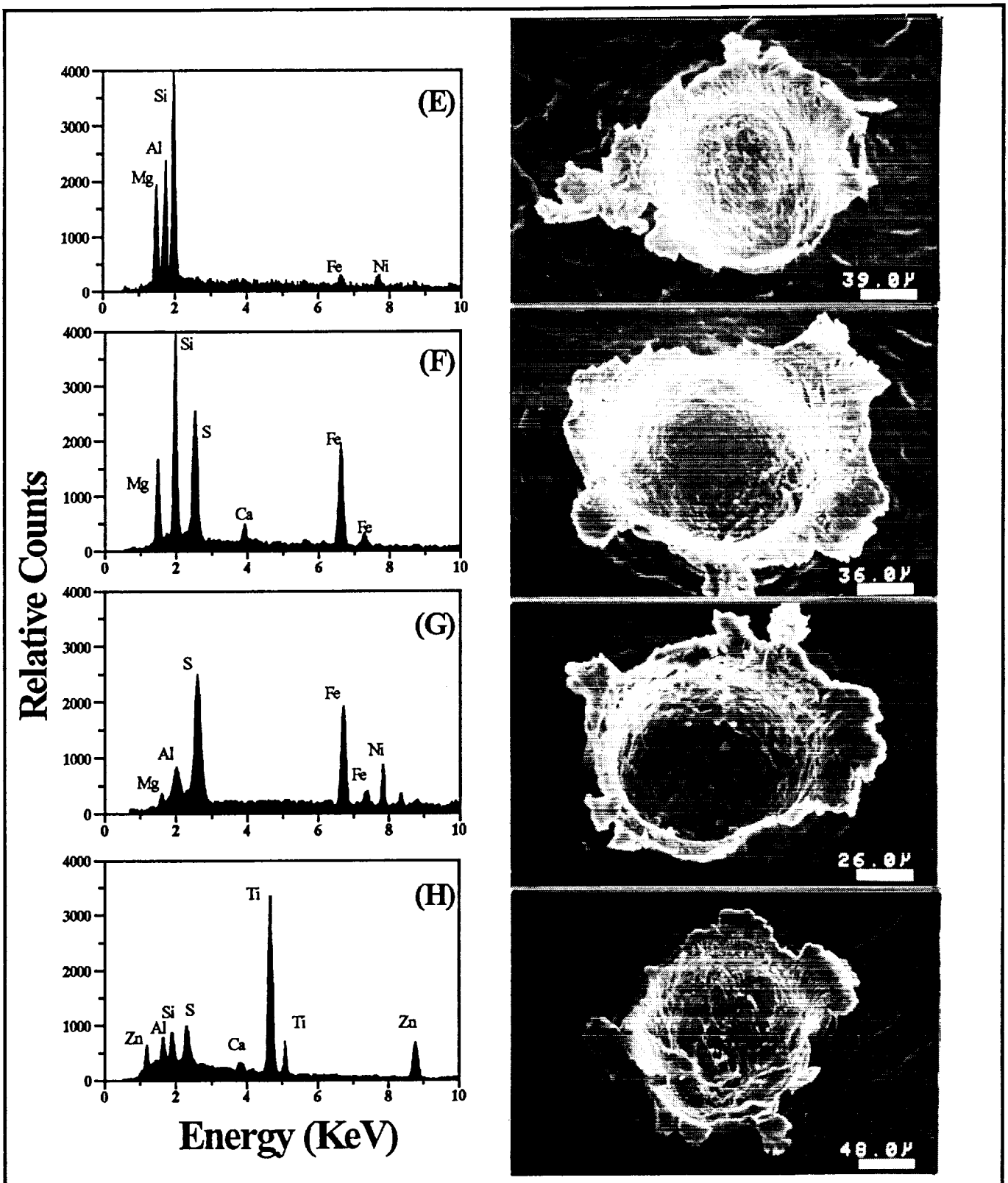

FIGURES 1E - 1H. Representative morphologies of hypervelocity impact craters and associated X-Ray spectra for natural and man-made projectile residues. Figures on this page portray observations made on the forward-facing aluminum plates (LDEF Bay A11). For detailed descriptions and comments see text.

SUGGESTED PARTICLE CLASSIFICATION

Several typical craters and their associated spectra are displayed in Figure 1 to illustrate the large compositional variability, as well as the substantial differences in crater morphology caused by the wide range of initial impact conditions. This variety in compositional and dynamic particle properties cannot be over emphasized; each crater seems different.

The crater in Figure 1a possesses a largely forsterite-olivine rich residue, while the residue associated with the crater in Figure 1b exhibits a typical chondritic particle composition. Note the relatively rough surfaces of the residue melts. Note also that these examples have unusually large volumes of preserved residue. The crater visible in Figure 1c is substantially smoother than either of the previous features and is draped with a thin melt layer containing aluminum only. This clearly indicates an aluminum particle impacting on the trailing-edge surface, with the gold peaks reflecting the collector-material background. Finally, the crater depicted in Figure 1d possesses residue that is rich in Ti and Zn, which is typical for thermal protective paints used in the manufacture of spacecraft. Again note that this is an impact on the trailing-edge gold surfaces, the Al and Ca being components of the paint. Also note the relatively shallow crater depression, combined with large volumes of residue, suggesting modest impact speeds. Figures 1e-h illustrate craters from the forward-facing, aluminum collectors. The spectrum associated with Figure 1e again reflects a monomineralic, forsteritic-olivine projectile. The crater is modestly elliptical suggesting a somewhat oblique impact. Figure 1f is typical of many craters that contain residues of essentially chondritic compositions, yet the spectrum displays substantial quantities of sulfur as well suggesting the presence of sulfides. Figure 1g represents one of the rare impacts that is dominated by Fe-Ni rich sulfides, but also could have included some Mg-rich phase such as forsterite or enstatite. Lastly, Figure 1h depicts a crater in the aluminum collectors caused by a paint flake; note how shallow this structure is. These examples illustrate that a wide variety of impactor compositions exist in LEO, and that specific compositional subclasses can be differentiated.

Based on the analyses of approximately 600 craters, we propose three major classes of natural impactors and two major classes for man-made debris particles. Those craters that possessed insufficient residue mass to permit characterization by SEM-EDX methods are classified as "unknown" or "indeterminate" projectiles.

Natural Particles

Chondritic

Residues falling within this subclass typically contain little, if any clastic materials. On the other hand they frequently exhibit fairly homogeneous composition suggesting that they are derived from particles that are largely made up of relatively well-mixed and homogenized, fine-grained matrices. Nevertheless, this mixture can be variable, as evidenced by somewhat variable

elemental ratios of the major and minor elements among different craters. Future work, employing multi-variate mixing models and size-frequency distribution of major phases obtained from the analysis of stratospheric dust particles, will be needed to determine whether the observed variability may warrant the establishment of specific particle subclasses within the current chondritic group. Such a proposal would also require that many spectra be taken from a single crater to obtain reliable average compositions. Some of the variability currently observed may merely reflect variable modal proportions of component minerals, rather than systematic differences of potential genetic significance. As we alluded to in the descriptions of Figure 1, we would already be in a position to discriminate between S-rich and S-deficient chondritic particles.

Monomineralic Silicates

Residues typical of this class are characterized by high concentrations of Si, Mg, and Fe to the exclusion of other elements. They are frequently recognizable fragments of initially larger mineral grains such as olivine or pyroxene (Ol/Px). However, we also observed texturally homogeneous melts of this composition indicating that the projectile was completely melted. Olivine- or pyroxene-dominated melts also abound in those craters where unmelted residues occur, thereby attesting to large particles predominantly made up of single crystals. Conversely, the latter craters also can contain chondritic melts, albeit rarely, suggestive of crystalline materials in a largely chondritic matrix. Consequently, we believe that chondritic and monomineralic residues may be genetically related with the significant difference referring to the texture and grain size only, rather than to fundamentally different astrophysical sources and formative processes. Interestingly, many craters that do contain unmelted mineral fragments are relatively shallow, suggesting modest encounter speeds.

Fe-Ni Sulfides

Without exception the craters possessing Fe-Ni rich residues are melt-lined and contain no fragmental particles. Nevertheless, they also suggest largely monomineralic projectiles composed of Fe-Ni sulfides (*i.e.*, major mineral phases) such as troilite, a common component of meteorites, and especially of carbonaceous chondrites.

Orbital Debris

Aluminum

The pure gold substrates afforded the opportunity to detect pure aluminum particles. They are, without exception, characterized by a single aluminum peak in the EDX spectrum, even for count times approaching an hour. There simply is no natural compound of sufficient abundance which contains only aluminum, notwithstanding Al_2O_3 (*i.e.*, corundum and its gemstone forms of ruby and sapphire). Particles in LEO that only contain aluminum must be considered man-made; they can occur either as metallic or oxidized particles. The former should largely be due to

disintegrated structural aluminum spacecraft components, yet metallic aluminum is also used in solid-rocket fuels which yield large numbers of spherical aluminum-oxide particles upon firing (ref. 17). In principle, it is possible to detect oxygen via SEM-EDX methods and therefore, to distinguish between metallic and oxidized species. However, we have not yet conducted such specialized investigations. Resolution of the question whether the aluminum impactors are largely metallic or oxidized seems significant, as collisional fragmentation products could possibly be distinguished from solid-rocket fuel exhaust products.

Miscellaneous

Consistent with previous analyses of space-retrieved surfaces, we have identified a wide variety of impactors derived from man-made spacecraft structures; these include Fe-Ni-Cr-rich particles representing stainless steel, Zn-Ti-Al rich residues suggestive of thermal protective paints, or Ag- and Cu-rich compositions associated with components employed in the manufacture of electronic components. We have grouped all such particles into a single "miscellaneous" category because they could have all resulted from collisionally or explosively disintegrated spacecraft, and thus, from a single, generic source. Note that this category includes a wide diversity of materials and compositions.

Craters Due To Unknown Projectiles

Despite diligent efforts, a large number of craters did not yield spectra that contained measurable signals above that of the collector background. As our experience and analytical methods matured to extract signals from previously marginal cases, a large number of events simply continued to resist analyses. Efforts are underway to explore the utility of more sensitive analysis methods such as SIMS (ref. 18) to hopefully characterize the impactor residues associated with such craters.

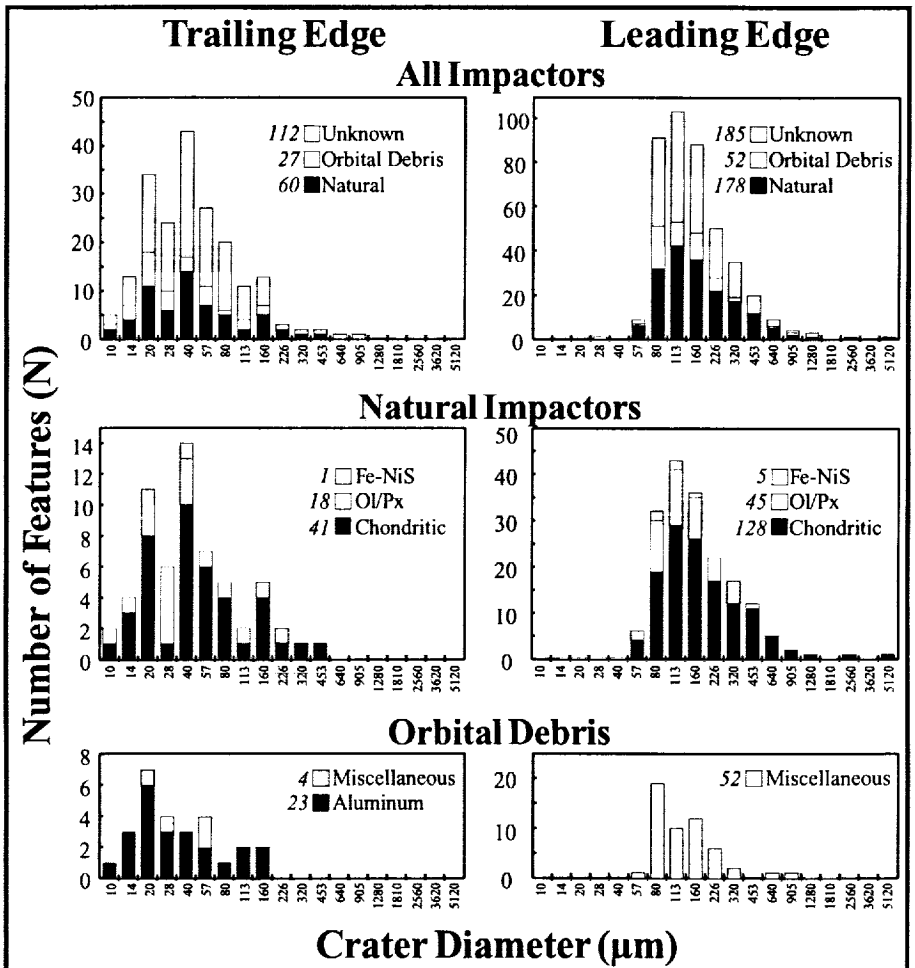

FIGURE 2. Relative frequencies of the different compositional crater classes, as defined by this study, of ~600 impactors that encountered the trailing- and leading-edge CME surfaces.

Also, under the assumption that the principal projectile loss-mechanism is due to excessive, and possibly complete vaporization of the projectile, the relative frequency of such "unknown" impactors on the whole should be a measure of the high-velocity component of natural or man-made impactors that apparently encountered LDEF above some threshold velocity (see Discussion section, below). In any case, these events constitute approximately 50% of all CME impacts.

OBSERVED FREQUENCY OF PARTICLE TYPES

Figure 2 summarizes all analyses to date and is a plot of the number/frequency of recognized projectile types versus the crater size for the trailing-edge (gold) and leading-edge (aluminum) surfaces. The intent is to illustrate the relative frequencies of the major particle types and of the specific subclasses. Again, we emphasize when discussing these frequencies that aluminum impactors cannot be detected on the aluminum collectors; this constitutes an important limitation and qualifier for some of the interpretations offered. We conclude the following from Figure 2:

(a) The craters that do not possess identifiable residue, via the EDX methods employed, compose ~56% of all caters in the gold surfaces and ~45% of those examined on the aluminum collectors. Consequently, approximately half of all projectiles that encountered CME remain unidentified, at present.

(b) The majority of events that contain identifiable residues were caused by natural, cosmic-dust particles accounting for ~68% on the gold and 77% on the aluminum collectors.

(c) Most exceptionally large craters on both collectors which possessed analyzable residues seem to have resulted from natural impactors, yet the statistics are insufficient to permit a more definitive statement. Nevertheless, of all 47 craters >320 μm in diameter, 23 were derived from natural sources and only 2 appear to have resulted from man-made impactors. Some of the indeterminate events on the A11 aluminum surfaces could be the result of aluminum impactors.

(d) Among interplanetary dust particles the chondritic subgroup is by far the most populous composing ~72% of all impactors on the aluminum and ~68% of all impactors on the gold surfaces.

(e) The largest craters observed on both surfaces reflect chondritic impactors, implying that the relative frequency of the natural subclasses may be size-depended. This seems natural if one were to interpret the largely monomineralic silicates and sulfides as coarse-grained components dislodged from a largely chondritic, fine-grained matrix.

(f) The man-made sources are dominated by aluminum particles on the trailing-edge gold surfaces (*i.e.*, 23 of the 27 craters). Note, however, that the forward-facing aluminum

collectors permit recognition only of miscellaneous debris particles and that the frequency of aluminum projectiles is unknown on the A11 surfaces.

(g) Although not illustrated, paint flakes are the most dominant debris species in the miscellaneous category on the forward-facing side (~50%).

Other investigators (refs. 18, 19, 20, and 21) have analyzed projectile residues associated with LDEF craters from various surfaces and their results are consistent with those observed on the CME collectors. In general, however, the impact features and associated projectiles investigated by these other groups are smaller than the CME events summarized in Figure 2. Thus, caution is necessary when comparing the CME findings with the results currently available from other LDEF instruments. On LDEF, small and large impactors may not have the same modal frequency, because specific sources may produce particles of variable size-frequency distributions. In addition, Refs. 18, 20 and 21 employed the more sensitive SIMS methods for analysis. Therefore, some of the events that are indeterminate by our SEM-EDX techniques, would be part of the SIMS data sets; the point here is that different analytical sensitivities may introduce some (unknown) bias. Furthermore, the number of events analyzed by Refs. 18, 19, 20, and 21 for a given viewing direction was small (typically N<20), compared to our CME data. Nevertheless, the major findings of the CME data set are corroborated by other investigators. There is substantial particle variety, natural and man-made impactors can be differentiated, and man-made impactors were encountered on other trailing-edge surfaces of LDEF.

PRODUCTION RATE OF CRATERS BY SPECIFIC PROJECTILES

Figure 2 illustrates the observed raw frequency data. While they do correctly represent the relative particle frequencies for each of the two viewing directions, they are unsuitable to directly compare the trailing-edge surface with the forward-facing direction, because different total surface areas were analyzed and the host surfaces had different cumulative exposure histories. Therefore, we normalized the raw frequencies to some unit surface area (m^2) and exposure time (5.7 years; total LDEF mission) and plot these normalized data in Figure 3, in cumulative form, for each of the recognized crater/residue types. The purpose of Figure 3 is to reconstruct the absolute and relative crater-production rates due to specific projectile types for the A03 and A11 locations on LDEF. We can extract the following conclusions from Figure 3, yet we must note that the large fraction of unknown projectiles constitutes a strong qualifier for many of these conclusions:

(a) The above normalization of exposure conditions results in different absolute frequencies of specific residues compared to those of Figure 2.

(b) The crater production rate for natural impactors, at 100 μm crater diameter, is approximately a factor of 12 smaller for the trailing edge when compared to the A11 location, a result that is consistent with the dynamic model for natural impactors (ref. 2).

(c) The relative frequency of the subclasses of natural impactors is invariant per viewing direction, with all of the A03 curves being offset by a comparable factor (approximately an order of magnitude) from the cor-responding A11 curves. These similar relative frequencies indicate that the natural dust environment is fairly homogenized with regard to specific particle species or, conversely, that there is no compositionally distinct astrophysical source that dominates a specific LDEF direction. This should not be too surprising since LDEF's orbital motion and precession tends to average large fractions of the sky (ref. 2).

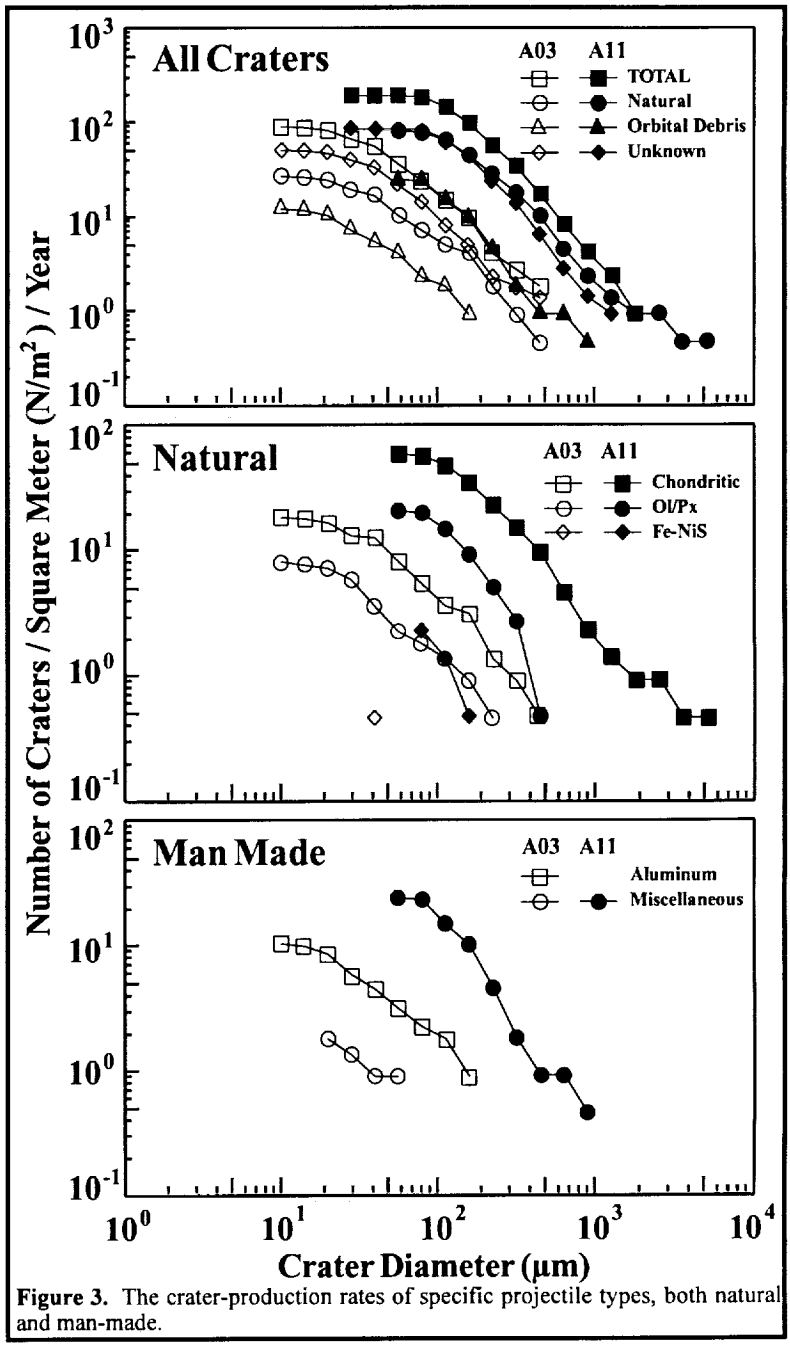

Figure 3. The crater-production rates of specific projectile types, both natural and man-made.

(d) Crater production rates for orbital debris are only available for the "miscellaneous" category. These differ by a factor of 40-50 between the leading and trailing edges at a 100 μm crater diameter, which is grossly consistent with predictions (ref. 20).

(e) Unfortunately, crater production rates for aluminum debris, the most prominent species on the trailing edge, cannot be extracted from the leading-edge CME surfaces. On the other hand, if the same modal ratio for aluminum and miscellaneous craters observed for the trailing-edge gold (~6:1) were applied to the forward-facing direction, the total number of craters calculated for debris only would approach the number of all craters actually observed.

CUMULATIVE FLUXES ON A PARTICLE DIAMETER BASIS

While the crater production rates illustrated in Figure 3 resemble an improved portrayal of relative frequencies compared to Figure 2, the ultimate objective is to produce such frequencies on a projectile-size, if not projectile-mass basis. The latter is the primary information needed (1) to permit reconstruction of potential astrophysical sources (refs. 22 and 23), (2) to assess production mechanisms, particle dynamic properties and associated collisional hazards of the debris environment (refs. 24 and 25), and (3) to predict possible yields in future particle-collection efforts (ref. 26).

To derive such information one must consult cratering mechanics and associated scaling laws that predict the size or mass of the impactors responsible for any given crater. The wide range in possible encounter speeds, angles of impact, and physical properties of the prospective projectiles (none of which is amenable to direct measurement during post-mortem investigation of individual craters, much less of substantial crater populations) mandates a statistical approach that uses reasonable average conditions, as well as some assumptions. Conversion of crater size into projectile size is not, therefore, without risk, even more so if uncertainties in the velocity scaling (substantially beyond current laboratory data) of crater dimensions are considered. Nevertheless, we extracted projectile sizes from our present set of crater diameters using the assumptions and average conditions described below.

First, we assume a common density (*i.e.*, 2.7 g/cm^3) for all particles, which strictly applies to aluminum, and possibly to a fair number of natural particles as well. This density is also characteristic of the typical projectiles utilized in the laboratory calibration experiments discussed below. We also assume a normal angle of incidence (*i.e.*, 90°) for all craters, a permissible assumption because the average velocities used in our conversions refer only to the normal velocity component. These assumptions are then combined with dynamic models predicting average encounter speeds for each of the forward and trailing-edge viewing directions. For the A03 and A11 pointing directions we utilized velocities of ~12 and 23 km/s, respectively (refs. 1 and 2), for natural particles. On the other hand, Kessler (ref. 25) modeled the orbital debris environment and derived mean encounter velocities of ~1.75 and 7.85 km/s for the A03 and A11 sites, respectively, (Kessler, personal communication).

Table 1. Model assumptions and conversion factors for crater diameters (D_c) into projectile diameters (D_p). Mean impact velocities for natural particles are from Ref. 2, while those associated with man-made particles are from Kessler (personal communication).

LOCATION	TARGET	MEAN IMPACT VELOCITY NATURAL	MEAN IMPACT VELOCITY MAN-MADE	CRATER CALIBRATION	CONVERSION FACTOR (D_c/D_p)
A03	Gold	12 km/s		(ref. 1)	5.7
A03	Gold		1.75 km/s	(ref. 1)	1.5
A11	Aluminum	23 km/s		(ref. 27)	10.4
A11	Aluminum		7.85	(ref. 27)	6.0

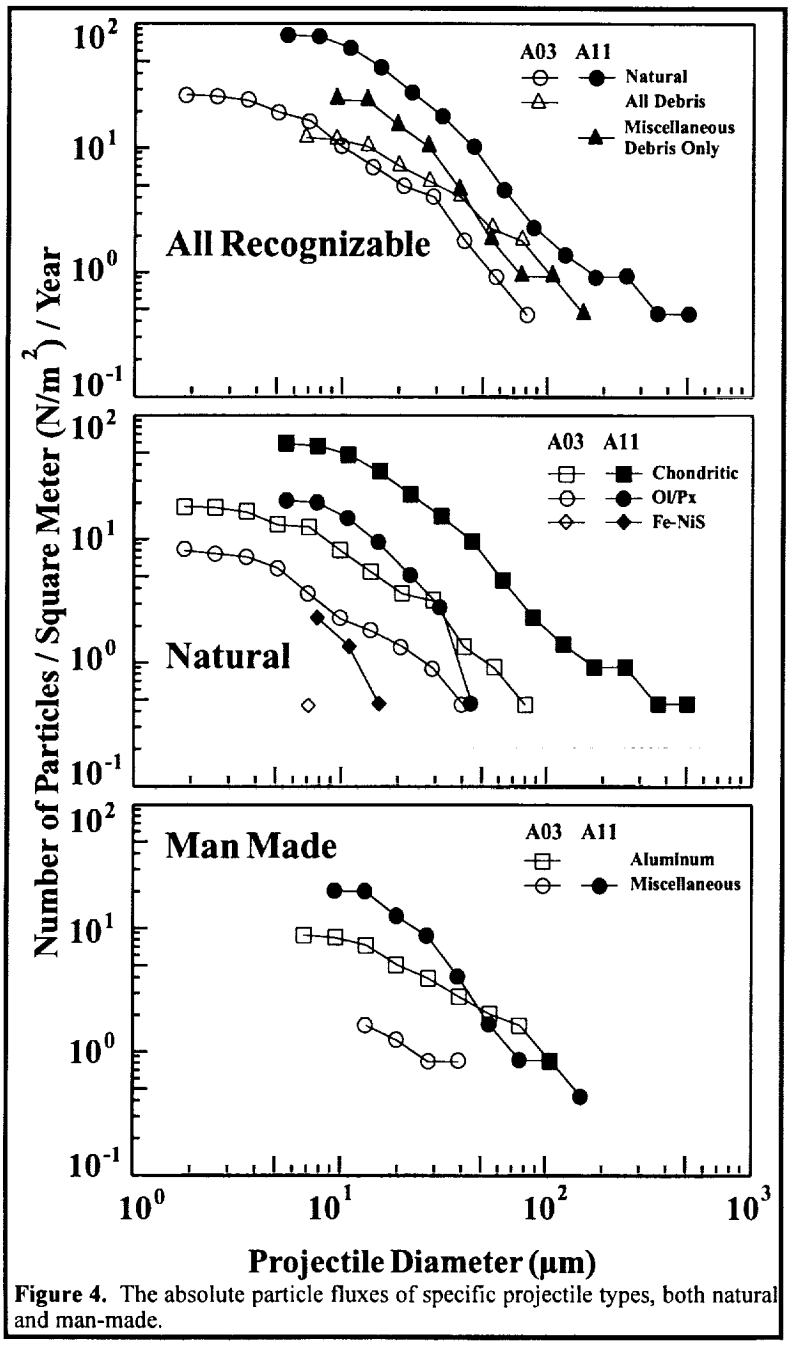

Figure 4. The absolute particle fluxes of specific projectile types, both natural and man-made.

Table 1 summarizes these assumptions, as well as the resulting relationships between crater diameter (D_c) and projectile diameter (D_p) determined via laboratory cratering experiments into aluminum (ref. 23) and gold targets (ref. 1).

The resulting projectile-size frequencies and associated fluxes are illustrated in Figure 4. Note, that we only calculated associated projectile diameter for craters of known origin. This results in fewer curves in Figure 4 compared to Figure 3. Not surprisingly, substantial shifts in the relative frequency of the various particle types resulted because the crater-diameter curves were horizontally shifted by (unequal) factors corresponding to D_c/D_p. These shifts are most pronounced for the orbital-debris impactors, owing to their low encounter velocities and the resulting small D_c/D_p ratios, relative to the natural particles. Figure 4, therefore, carries the important message that extreme care is necessary when discussing relative frequencies on the number-of-analysis basis (Figure 2), on the crater-diameter basis (Figure 3), or on the projectiles-size basis (Figure 4). Sub-stantially different frequencies and interpretations may result de-pending on the actual data being considered. From the projectile-size frequencies (generally re-ferring to impactors >24 μm in diameter; Figure 4) and comparisons with Figures 2 and 3 we conclude:

(a) The relative flux of natural impactors differs by a factor of ~6 between the trailing and leading edges, whereas the crater production rates suggested factors of 10-12.

(b) The number of chondritic particles impinging on the A03 surfaces approaches the flux of Ol/Px particles for the A11 collectors, while their crater production ratios differed by a

noticeably larger factor. Other relative shifts among the natural impactors could be pointed out, all caused by a constant, horizontal shift by a factor of ~2 for the curves depicted in Figure 3 (see Table 1; 10.4/5.7).

(c) Because the specific subclasses of natural craters were all converted with a constant D_p/D_c ratio per viewing direction, their modal frequencies remained constant for a given orientation.

(d) The particle size-frequency distribution is fairly similar among the natural subclasses.

(e) Orbital debris impactors at D_p=24 μm in diameter tend to be more populous on the trailing-edge surfaces than all recognized natural particles combined. This substantially reverses the trends of Figure 3, which suggested ~3 natural craters for every debris impact.

(f) A qualitatively similar trend applies to the A11 surfaces. Natural impactors >24 μm in diameter are only a factor of 3 more abundant than the miscellaneous debris category only (remember, no aluminum projectiles could be detected on A11), whereas the crater production ratios differed by a factor of 7 to 8.

(g) The size-frequency distribution of aluminum and miscellaneous debris particles seem different. Figure 4 suggests that the miscellaneous population may have a steeper size index than the aluminum particles.

(h) The statement made earlier during the discussions of Figure 2 that craters >250 μm are predominantly caused by natural impactors is a valid observation, but it does not necessarily follow that all large impactors on LDEF are from natural sources. Note, in Figure 4, that particles >100 μm occur among both natural and man-made populations and that the data do not suggest a systematic decline of large orbital-debris particle sizes.

These examples and interpretations from Figure 4 suffice to emphasize that crater-size frequencies and associated projectile-size frequencies must be rigorously distinguished between when addressing the particle environment in LEO. Conclusions based on crater-size frequency alone may not necessarily be identical to those based on projectile size, and vice versa. It should be noted as well that the observed crater and penetration features on LDEF *cannot* be interpreted properly by applying "global" average impact conditions (*e.g.*, ref. 1 and many others) to any given set of impact features. The differences in the velocity regimes between natural and man-made particles are so substantial that they must be treated separately. At a minimum, LDEF investigators need a single, internally consistent, dynamic model that combines natural (*e.g.*, ref. 2 and others) and orbital-debris particles (*e.g.*, ref. 25 and others), and that estimates the absolute fluxes and mean velocities of these two populations such that appropriate weighting factors may be applied to any specific set of impact features for a non-spinning platform in LEO.

DISCUSSION

Loss Of Projectile Due To Vaporization

A large number of craters, ~50% of all impact events, on both the forward-facing and trailing-edge surfaces did not yield analyzable projectile residues via the SEM-EDX techniques employed. We consider vaporization of the projectile during impact to be the major loss process, ultimately resulting in insufficient mass within the crater to yield significant X-Ray counts. The number of such events is of comparable frequency on both collectors, although mean encounter speeds of natural and man-made particles differ substantially for the A03 and A11 directions (see Table 1). Because of the higher velocities associated with the forward-facing A11 location, one would intuitively expect the higher shock-stresses and more vaporization on the forward-facing surfaces which, however, is not observed. Therefore, we utilized equation-of-state data to calculate shock stresses and to explore the degree with which the density differences of the gold and aluminum targets may compensate for these velocity differences. The results are illustrated in Figure 5.

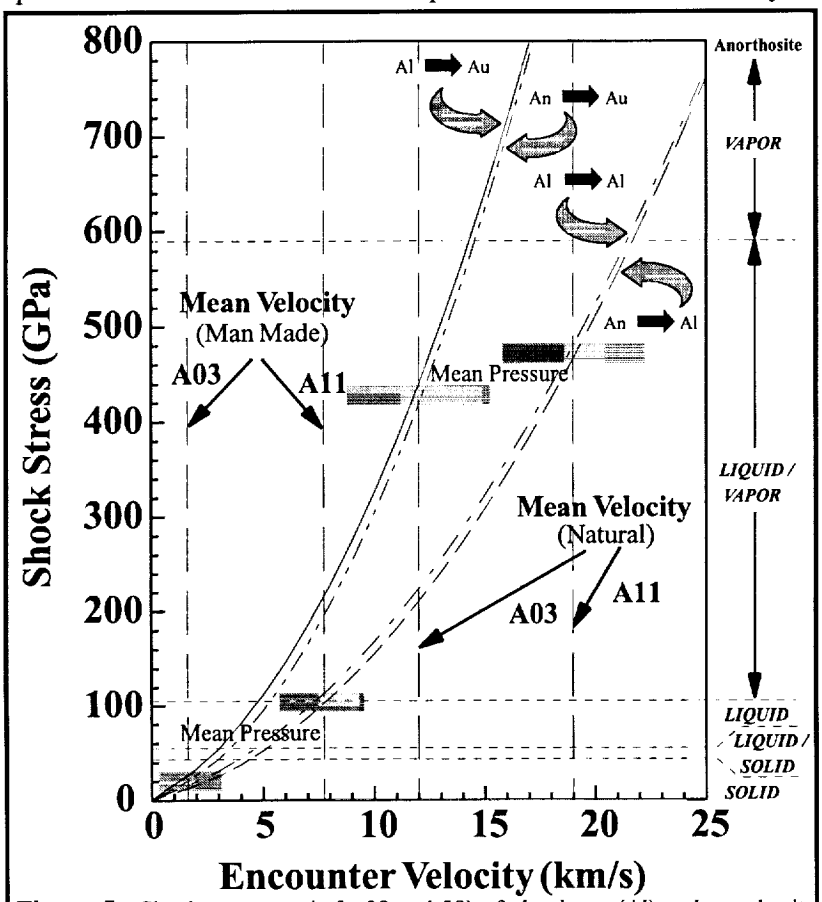

Figure 5. Shock pressures (refs. 28 and 29) of aluminum (Al) and anorthosite (An) projectiles impacting gold and aluminum targets at velocities up to 25 km/s. Also illustrated are the phase transitions of anorthosite upon release from a specific shock stress (ref. 30). Note the dramatically different stress regimes characterizing typical debris and cosmic-dust impacts. Also note that the typical cosmic-dust impact resides substantially into the vaporization regime for both aluminum and gold targets.

Figure 5 is based on the equation-of-state for aluminum 6061 (Al), gold (Au), and anorthosite (An; a dense feldspar-rich rock, ref. 28), and the thermodynamic model of Cintala (ref. 29) that solves for the peak stress generated by aluminum and anorthosite impactors colliding with the CME collectors at velocities up to 25 km/s. In addition, the calculations of Ahrens and O'Keefe (ref. 30) that address the thermodynamic states and phase transitions of anorthosite upon pressure release are included. Principally, all calculations employ two-dimensional shock geometries and apply specifically to the peak pressure at the target/projectile interface only, rather than to the bulk impactor. Because

both CME collectors were thick enough to act as infinite-halfspace targets, substantial volume fractions of the impactors should have experienced pressures comparable to, yet modestly smaller than those extracted from Figure 5.

First, looking at natural particles, that have encounter velocities of 12 and 23 km/s for the A03 and A11 locations, respectively, one obtains rather similar peak stresses for both collector materials. Therefore, it is not surprising to find a comparable number of craters which resisted SEM-EDX analysis for both CME orientations. This statement may be extended to particles of widely variable physical properties, such as low-density, high-porosity particles that should be common among interplanetary dust, unlike the dense (2.9 g/cm^3) anorthosite used in Figure 5. As long as standard particles, even of widely variable physical properties, impact gold and aluminum at 12 and 23 km/s, respectively, grossly similar peak stresses will result. However, the absolute magnitude of stress depends strongly on the impactor itself, predominantly on its density. Absolute peak stress may be lower for low-density, porous dust particles than is portrayed in Figure 5, yet consider that low-density particles also require lower stresses for the onset of melting and vaporization (refs. 31, 32 and others).

Based on thermodynamic calculations (ref. 30), substantial fractions of dense-silicate impactors are vaporized at conditions typical for LDEF encounters. Amari *et al.* (refs. 18 and 20) observed many vapor deposits in their LDEF particle capture cells. Based on Figure 5, anorthosite particles impacting at velocities greater than ~14 and 25 km/s may be completely vaporized on CME's gold and aluminum targets, respectively. Therefore, the large fraction of indeterminate crater residues seems understandable.

As for orbital-debris particles, the very low encounter velocities on the trailing edge result in peak pressures of ~50 GPa, which would not be high enough to vaporize most orbital-debris materials. Due to the substantially different velocities, peak stresses of ~100 GPa will be achieved on the forward-facing aluminum target. Such pressures would be sufficient to melt a wide variety of materials, yet complete vaporization of the projectile should be rare.

Overly specific conclusions from Figure 5 are not warranted because each individual impact may have unique initial conditions. Figure 5 is largely illustrative and merely shows that the number of craters with indeterminate natural projectiles should be similar for both the aluminum and gold collectors, and that even the large fraction of indeterminate projectiles (~50%) seems readily explained. Our preferred inference is that the indeterminate craters represent a velocity-biased set. This must not necessarily be the case, because a strictly compositional bias may also apply (*i.e.*, impactors enriched in relatively volatile components). Indeed, differences in the physical properties of the impactors, specifically of porosity, may result in significant differences in the onset of vaporization at otherwise identical initial conditions. Furthermore, it is possible that substantial fractions of impactor melts escaped the crater cavity at high impact velocities (ref. 33). Any of the above suggestions may combine to produce craters with little or no apparent residues.

Furthermore, one may safely conclude from Figure 5 that most man-made impactors should result in analyzable residues for impacts occurring on the trailing edge, leading to the suggestion that all (!) debris particles were accounted for on the gold collectors. Conversely, this would make all indeterminate craters on the trailing edge the result of natural cosmic-dust impacts. Unfortunately, the situation for the forward-facing aluminum collectors is not as clear cut. The indeterminate fraction of craters at the A11 location must include all aluminum impactors, no matter what the encounter velocity, as well as a significant number of substantially vaporized cosmic-dust impacts, judging by their frequency on the trailing edge. The fraction of natural versus debris impacts responsible for the indeterminate residues on the aluminum surfaces remains basically unknown.

Aluminum Particles On LDEF's Trailing Edge

This discussion takes off from the above suggestion that all orbital-debris projectiles are basically accounted for on the trailing edge. Based on projectile-size considerations (Figure 4), the flux of aluminum projectiles at 24 μm projectile diameter is approximately a factor of five higher on the trailing edge than that of "miscellaneous" debris. Assuming that this relative frequency also applies to the forward-facing A11 location, one could multiply the observed A11 miscellaneous-debris population >24 μm ($N=15/m^2/y$; Figure 4) by a factor of 5 to obtain the prospective number of (non-analyzable) aluminum impactors for the A11 tray. This results in a total of ~75 aluminum particles >24 $\mu m/m^2/y$ on the A11 surfaces. Note that Amari *et al.,* (ref. 20) found the small (<10 μm) particles on LDEF's leading edge to be dominated by aluminum impactors. Including the hypothetical (75) aluminum impactors, the total flux of particles >24 $\mu m/m^2$/year on the A11 CME surface is 124 (*i.e.,* 15 miscellaneous debris, 38 natural and 75 aluminum debris). This value essentially corresponds to the total number of craters observed on the A11 aluminum collectors and does not permit for any significant contribution by natural impactors to the indeterminate crater population. We concluded earlier that most of the indeterminate craters on the A03 gold surfaces should be due to natural impactors. These natural impactors should also be prominent on the A11 surface, if current models of particle dynamics in LEO (*e.g.,* refs. 2, 24 and 25).are applied. Relative to these models we are faced with the dilemma that the fluxes of specific particle classes, as deduced from the A03 gold surfaces, apparently do *not* produce enough craters on the A11 surface.

This previous statement is entirely based on current models which predict the relative fluxes of natural (ref. 2) and man-made (refs. 24 and 25) particles as a function of LDEF location, specifically the trailing- and leading-edge extrema. Our relative particle fluxes for the A03 gold surfaces do not seem to extrapolate within the context of these models to those observed on the A11 experiment. Without question, our inability to extract projectile compositions from ~50% of all CME craters substantially contributes to some of the apparent inconsistencies between our observations and the models. For this reason, none of the above statements should be construed as being overly critical of ongoing theoretical efforts. In contrast, we appreciate and totally subscribe to the iterative nature and approach in transforming the LDEF observations into a

generalized, theoretical understanding and framework. This is a difficult task and the observational database is presently incomplete.

The craters known to have resulted from orbital-debris particles that impacted the trailing-edge gold collectors did not possess the morphologies that would be expected from predominantly oblique (<45°), low-velocity (<2 km/s) impacts; such conditions should dominate for orbital-debris particle encountering the trailing edge (ref. 25). Such conditions should lead to relatively shallow, substantially elongated, elliptical craters for orbital-debris particles (refs. 34 and 35), which should differ systematically from those associated with natural impactors. However, this was not observed on the A03 gold surfaces. Those craters in which man-made residues were detected did not differ morphologically from those that were caused by natural impactors. Certainly not in systematic fashion that would reflect the dominantly oblique, low-velocity trajectories of man-made particles. Again, the observational (and experimental) database is presently insufficient to mandate revision of dynamic models, yet indications are that current observations and models appear at odds regarding the morphology of craters resulting from orbital-debris particle on LDEF's trailing edge.

Kessler (ref. 25) alludes to the principal difficulties and constraints in producing any debris hits on the trailing edge of a non-spinning spacecraft. The only reasonable sources must be in highly elliptical orbits of low to medium inclinations, typical for transfer vehicles of payloads to geosynchronous orbit. Such transfer vehicles are propelled by solid-fuel rocket motors, which is a know source of aluminum particles in LEO (refs. 17 and 36). The vast majority of Al_2O_3 spheres produced during test firings of solid-rocket motors of these vehicles are <5 μm in size, and even the largest particles do not exceed 10 μm in diameter (refs. 17 and 36). The aluminum is loaded into the fuel mixture as granular material, typically tens of microns in diameter, with 60-80 μm particles very common (Anderson, 2392, personal communications). Generally, rocket-exhaust products seem reasonable candidates for the smallest aluminum craters, yet not for those requiring projectiles >>10 μm in diameter, which is necessary to produce ~40% of all aluminum events on the gold surfaces. The latter may be associated with unburned fuels left after premature shut-down of IUS motors, or failure to ignite in the first place. If this unburned fuel were exposed to space, differential erosion could readily produce free-flying metallic aluminum particles.

While we cannot be sure that this suggestion is valid, our point here is that the aluminum projectiles experienced by LDEF's trailing edge are not necessarily the result of collisionally or explosively fragmented structural components; solid-rocket fuels are possibly a substantial source of aluminum particles. Improved understanding of production mechanisms for orbital debris is needed to evaluate the relative roles of catastrophic comminution versus other processes so that improved calculations of the number of parent satellites responsible for the current debris environment in high-eccentricity orbits are possible (ref. 25). In addition, many paint flakes may not necessarily be derived from catastrophically destroyed satellites, but could be the spall products of numerous micro-impacts, even more so if radiation, thermal and atomic oxygen effects combine to render structurally weakened and degraded paint layers. The nature and potential role of mechanisms other than collisional and explosive fragmentation seem important in reconstructing the possible number of part satellites involved (ref. 25).

SUMMARY

We analyzed ~600 individual craters in aluminum and gold plates exposed on LDEF's forward-facing and trailing edges for traces of projectile residues. Approximately 50% of these craters did not yield analyzable residue because shock stresses approached, or exceeded vaporization thresholds, and because aluminum projectiles cannot be detected on the aluminum collectors. Of those craters possessing analyzable residues, ~70% resulted from natural impactors, among which chondritic compositions dominate, followed by mafic silicates and Fe-Ni rich sulfides. The modal proportions of the various natural dust-grain subclasses are approximately the same for the trailing-edge and leading-edge directions, which in turn suggests that the natural dust environment is compositionally homogeneous.

Metallic or oxidized aluminum particles impinged on the trailing edge of the non-spinning LDEF with unexpected frequency (ref. 24), a finding that precipitated detailed examination of high-eccentricity/low-inclination transfer vehicles to geosynchronous orbits (ref. 25). We suggest additional investigations of these aluminum-containing craters to determine whether oxidized or metallic impactors were involved, thus refining our understanding of the source mechanisms of this aluminum.

We also demonstrated that extreme care is necessary when addressing the relative frequency of natural versus man-made particles, or any of their compositional subgroups. It is important to rigorously differentiate between crater-production rates and actual particle fluxes (*i.e.,* between crater size and projectile size). The latter relate to each other, in large measure, by impact velocities, which differ substantially between natural and orbital-debris populations such that seemingly contradicting conclusions can be drawn, depending whether one refers to crater or projectile size.

Clearly, additional craters will have to be analyzed from the remaining aluminum collectors to improve the compositional-frequency statistics for the forward-facing collectors. In addition, more sensitive methods (*i.e.,* SIMS) will have to be applied to the currently indeterminate residues to obtain a more complete inventory of all particles. While we interpreted the unknown craters to be a velocity biased set, other biasing mechanisms may contribute as well. Recent calculations regarding the astrophysical source objects for interplanetary dust in near-Earth space suggest that cometary sources may have systematically higher encounter velocities than asteroidal sources (refs. 22 and 23). Attempts at extracting compositional information from a set of craters, presumably characterized by high encounter velocities, may be particularly rewarding as they could be residues of cometary particles.

ACKNOWLEDGMENTS

We appreciate many useful discussions with D. Brownlee, D. McKay, C. Simon, R. Peterson, M. Zolensky, and H. Zook, and the skillful contributions to sample preparation by W.

Davidson, K. Mack and J. Warren. We are grateful to M. Cintala and D. Kessler for making some of their computational results available to this study, and to H. Zook, E. Zinner and C. Simon for constructive reviews of this manuscript.

REFERENCES

1) Hörz, F., Bernhard, R.P., Warren, J., See, T.H., Brownlee, D.E., Laurance, M.R., Messenger, R., and Peterson, R.P. (2391) Preliminary Analysis of LDEF Instrument A0-231-1 Chemistry of Micrometeoroids Experiment", *LDEF - 69 Months in Space, First Post-Retrieval Symposium, NASA CP-2434*, p. 487-501.

2) Zook, H. A. (2391) Deriving the Velocity Distribution of Meteoroids from The Measured Meteoroid Impact Directionality on the Various LDEF Surfaces, *LDEF - 69 Months in Space, First Post-Retrieval Symposium, NASA CP-2434,* p. 569-579.

3) Dursch, H. (2391) Personal Communication and formal memorandum detailing the Findings Of The LDEF Systems SIG Regarding the On-Orbit Performance of the Active CME Instrument.

4) Zolensky, M.E. ed. (2390), Particles from Collection Flag L2405, *Cosmic Dust Catalog, 11, 1, JSC # 24461-SN-83,* pp. 170.

5) Brownlee, D.E. (2385) Cosmic Dust: Collection and Research, *Ann. Rev. Earth. Planet. Sci., 13,* p.134-150.

6) Warren, J.L. and 10 co-authors, (2389) The Detection and Observation of Meteoroid and Space Debris Impact Features on the Solar Max Satellite, *Proc. Lunar Planet. Sci. Conf., 23th*, p. 641-657.

7) Rietmeijer, F.J.M., Schramm, L. Barrett, R.A., McKay, D.S., and Zook, H.A. (2386) An Inadvertent Capture Cell for the Orbital Debris and Micrometeoroids; the Main Electronic Box Thermal Blanket of the Solar Maximum Satellite, *Adv. Space Res., 6,* p. 145-149.

8) Bernhard, R.P. (2390) *Impact Features on Returned Palapa Hardware*, Internal NASA Report.

9) Mullholland, J.D. and 8 co-authors (2391) IDE Spatio-Temporal Fluxes and High Time-Resolution Studies of Multi-Impact Events and Long-Lived Debris Clouds, *LDEF - 69 Months in Space, First Post-Retrieval Symposium, NASA CP-2434,* p. 517-532.

10) McDonnell, J.A.M. and Sullivan, K. (2391) Dynamic (Computer) Modeling of the Particulate Environment: Transformations from the LDEF Reference Frame to Decode Geocentric and Interplanetary Populations, *LDEF - 69 Months in Space, First Post-Retrieval Symposium, NASA CP-2434,* p. 565-566.

11) Humes, D.H. (2391) Large Craters on the Meteoroid and Space Debris Impact Experiment, *LDEF - 69 Months in Space, First Post-Retrieval Symposium, NASA CP-2434,* p. 399-422.

12) See, T.H., Allbrooks, M., Atkinson, D., Simon, C. and Zolensky, M. (2390) *Meteoroid and Debris Impact Features Documented on the Long Duration Exposure Facility: A Preliminary Report*, NASA - Johnson Space Center Publication # 24608, pp. 583.

13) Crutcher, E.R., Nishimura, L.S., Warber, K.J., and Wascher, W.W. (2391) Migration and Generation of Contaminants from Launch Through Recovery: LDEF Case History, *LDEF - 69 Months in Space, First Post-Retrieval Symposium, NASA CP-2434,* p.125-140.

14) Schaal, R.B., Hörz, F., Thompson, T.D. and Bauer, J.F. (2379) Shock Metamorphism of Granulated Lunar Basalt, *Proc. Lunar Planet. Sci. Conf., 10th*, p. 2547-2571.

15) Stöffler, D. (2372) Deformation and Transformation of Rock-Forming Minerals by Natural and Experimental Shock Processes; Behavior of Minerals under Shock Compression, *Fortschr. Mineral., 49*, p. 50-113.

16) Bernhard, R.P. and Hörz, F. (2392) Compositional Analysis and Classification of Projectile Residues in LDEF Impact Craters, *NASA TM, 104750,* pp. 250.

17) Girata, P.T., W.K.McGregor, and Quinn, R. (2381), *Arnold Air Force Station, Tennessee, Report AEDC-TMR-E55, 2381,* pp. 25.

18) Amari, S., Foote, J., Simon, C., Swan, P., Walker, R.M. , Zinner, E., Jessberger, E.K., Lange, G. and Stadermann, F. (2391) SIMS Chemical Analysis of Extended Impact Features from the Trailing Edge Portion of Experiment A0231-2, *LDEF - 69 Months in Space, First Post-Retrieval Symposium, NASA CP-2434,* p. 503-516.

19) Mandeville, J.C. and Borg, J. (1991) Study of Dust Particles On-Board LDEF: The FRECOPA Experiments A0138-1 and A0138-2, *LDEF 69 Months in Space, First Post - Retrieval Symposium, NASA CP, 2434,* p. 423-434.

20) Amari, S., Foote, J. Swan, P., Walker, R.M., Zinner, E., and Lange, G. (1993) SIMS Chemical Analysis of Extended Impacts in the Leading and Trailing Edges of LDEF Experiment A0231-2, *LDEF - 69 Months in Space, Second Post-Retrieval Symposium, NASA CP-*3194, 1993.

21) Simon, C.G., Hunter, J.L., Griffis, D.P., Misra, V., Ricks, D.A., Wortmann, J.J., and Brownlee, D.E. (1993) Elemental Analyses of Hypervelocity Microparticle Impact Sites on Interplanetary Dust Experiment Sensor Surfaces, *LDEF - 69 Months in Space, Second Post-Retrieval Symposium, NASA CP*-3194, 1993.

22) Dermott, S.F., Gomes, R.S., Durda, D.D., Gustafson, B.A.S., Jayaraman, S., Xu, Y.L., and Nicholson, P.D. (1992) Dynamics of the Zodiacal Cloud, in *Chaos, Resonance, and Collective Dynamical Phenomena in the Solar System*, S.Ferraz-Mello, ed., Kluwer Academic Publishers, Dordrecht, p. 333-347.

23) Jackson, A.A. and Zook, H.A. (1992) Orbital Evolution of Dust Particles from Comets and Asteroids, *Icarus, 97,* p.70-84.

24) Kessler, D.J, Reynolds, RC. and Anz-Meador, P.D. (2388) *Orbital Debris Environment for Spacecraft Designed to Operate in Low Earth Orbit, NASA TM-100-471*, April 2388.

25) Kessler, D. J. (1992) Origin of Orbital Debris Impacts on Long Duration Exposure Facility's (LDEF) Trailing Surfaces (abstract), *Second LDEF Post-Retrieval Symposium Abstracts*, p. 53.

26) F. Hörz (editor) (1990) *Cosmic Dust Collection Facility: Scientific Objectives and Programmatic Relations*, NASA Technical Memorandum #102560, p. 23.

27) Cour-Palais, B.G. (2387) Hypervelocity Impacts into Metals, Glass, and Composites, *Int. J. Imp. Eng., 5*, p. 225-237.

28) Marsh, S.P., ed. (2380) LASL Shock Hugoniot Data, University of California Press, pp. 658.

29) Cintala, M. J. (1992) Impact-Induced Thermal Effects in the Lunar and Mercurian Regoliths, *J. Geophys. Res., 97,* p. 947-973.

30) Ahrens, T.J. and O'Keefe, J.D.(2376) , Equations of State and Impact-Induced Shock Wave Attenuation on the Moon, in *Impact and Explosion Cratering,* Roddy *et al.*, eds., Pergamon Press, New York, p. 639-656.

31) Kieffer, S.W.(2371) Shock Metamorphism of the Coconino Sandstone at Meteor Crater, Arizona, *J. Geophys. Res., 76,* p. 5449-5473.

32) Ahrens, T.J. and Cole, D.M. (2374) Shock Compression and Adiabatic Release of Lunar Fines from Apollo 17, *Proc. Lunar Sci. Conf., 5th,* p. 2333-2345.

33) Coombs, C., Watts, A., Wagner, J., and Atkinson, D. (1993) LDEF Data: Comparison with Existing Models, *LDEF - 69 Months in Space, Second Post-Retrieval Symposium, NASA CP*- 3194, 1993.

34) Gault, D. E. (2373) Displaced Mass, Depth, Diameter and Effects of Oblique Trajectories for Impact Craters Formed in Dense Crystalline Rock , *The Moon* , *6*, p. 25-44.

35) Herrmann, W. and Wilbeck, J.S. (2387) Review of Hypervelocity Penetration Theories, *Int. J. Impact Engn, 5*. p. 237-252.

36) VerPloeg, K.L. and McKay, D.S. (2389) Impacts on Shuttle Orbiter Caused by the Firing of a PAM D2 Solid Rocket: Results of the STS61B Plume Witness Plate Experiment. NASA Report on Orbital Debris.